BIOCHEMISTRY
including biophysical chemistry & molecular biology

Article

pubs.acs.org/biochemistry

Quinone Reductase 2 Is an Adventitious Target of Protein Kinase CK2 Inhibitors TBBz (TBI) and DMAT

Kevin K. K. Leung and Brian H. Shilton*

Department of Biochemistry, University of Western Ontario, London, Ontario, Canada N6A 5C1

ABSTRACT: Quinone reductase 2 (NQO2) exhibits off-target interactions with two protein kinase CK2 inhibitors, 4,5,6,7-1*H*-tetrabromobenzimidazole (TBBz) and 2-dimethylamino-4,5,6,7-tetrabromo-1*H*-benzimidazole (DMAT). TBBz and DMAT induce apoptosis in cells expressing an inhibitor-resistant CK2, suggesting that the interaction with NQO2 may mediate some of their pharmacological effects. In this study, we have fully characterized the binding of TBBz and DMAT to NQO2. Fluorescence titrations showed that TBBz and DMAT bind oxidized NQO2 in the low nanomolar range; in the case of TBBz, the affinity for NQO2 was 40-fold greater than its affinity for CK2. A related CK2 inhibitor, 4,5,6,7-tetrabromobenzotriazole (TBB), which failed to cause apoptosis in cells expressing inhibitor-resistant CK2, binds NQO2 with an affinity 1000-fold lower than those of TBBz and DMAT. Kinetic analysis indicated that DMAT inhibits NQO2 by binding with similar affinities to the oxidized and reduced forms. Crystal structure analysis showed that DMAT binds reduced NQO2 in a manner different from that in the oxidized state. In oxidized NQO2, TBBz and DMAT are deeply buried in the active site and make direct hydrogen and halogen bonds to the enzyme. In reduced NQO2, DMAT occupies a more peripheral region and hydrogen and halogen bonds with the enzyme are mediated through three water molecules. Therefore, although TBB, TBBz, and DMAT are all potent inhibitors of CK2, they exhibit different activity profiles toward NQO2. We conclude that the active site of NQO2 is fundamentally different from the ATP binding site of CK2 and the inhibition of NQO2 by CK2 inhibitors is adventitious.

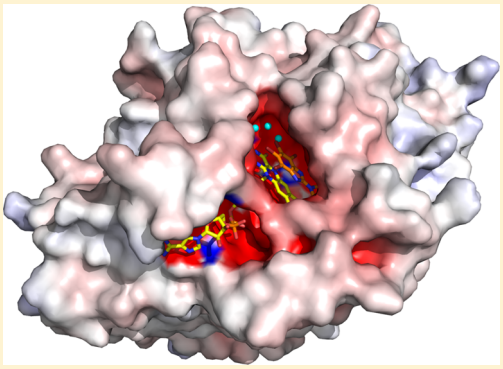

Protein kinases are often deregulated in cancer, and the development of kinase inhibitors for cancer chemotherapy has received much attention in the past 30 years.[1] Protein kinase CK2 (CK2) is a constitutively active kinase that phosphorylates more than 200 protein targets and regulates a myriad of cell signaling events in cell cycle, apoptosis, and transcriptional control.[2,3] With regard to apoptosis, CK2 attenuates cell death by phosphorylation of caspases and caspase targets.[4] Therefore, the overexpression of CK2 in many tumor types suggests that CK2 is involved in tumorigenesis by preventing cell death.[5] As such, CK2 is an attractive cancer therapy target and CK2 inhibitors that cause apoptosis in cancer cells have been extensively developed over the past two decades.[6] However, despite tremendous efforts to increase the specificity of inhibitors for CK2, many of these compounds exhibit off-target interactions.

The tetrabromobenzene compounds 4,5,6,7-tetrabromobenzotriazole (TBB), 4,5,6,7-tetrabromobenzimidazole (TBBz), and 2-dimethylamino-4,5,6,7-tetrabromo-1*H*-benzimidazole (DMAT) are some of the most widely used inhibitors of CK2 (Figure 1). TBB inhibits CK2 activity in the submicromolar range with relatively high specificity over other kinases,[7−9] and treatment of cells in culture with TBB leads to apoptosis.[10] Further development of TBB led to the discovery of another potent inhibitor of CK2, TBBz, that is more selective for yeast CK2.[11,12] Based on the tetrabromobenzene moiety in TBBz, another CK2 inhibitor, DMAT, was developed that was more selective for CK2 than TBB and bound with an affinity 10-fold greater than that of either TBB or TBBz.[13,14] Despite being optimized for CK2 inhibition, both TBBz and DMAT inhibit at least three other subfamilies of kinases: DYRKs, PIM, and HIPK2.[15] Furthermore, they also bind several non-kinase targets with ATP binding sites.[16] Such nontargeted interactions may contribute to the cellular effects of the inhibitors.

In a series of unbiased validation studies of the specificity of these inhibitors, Duncan and co-workers identified quinone reductase 2 (NQO2) as a particularly interesting non-kinase target of TBBz and DMAT.[17] Briefly, an inhibitor-resistant mutant of CK2 was transfected into cells to rescue them from CK2 inhibitor-induced apoptosis; however, only TBB-treated cells were rescued, while TBBz- and DMAT-treated cells underwent apoptosis. Therefore, inhibition of CK2 alone did not fully account for the cell death caused by TBBz and DMAT treatment. This challenges the notion that CK2 is the bona fide target of the two inhibitors and indicates that TBBz and DMAT act through alternate mechanisms to cause cellular apoptosis. Further investigation using a proteomics approach identified a

Special Issue: New Frontiers in Kinases

Received: August 2, 2014
Revised: November 4, 2014
Published: November 7, 2014

   dx.doi.org/10.1021/bi500959t | *Biochemistry* 2015, 54, 47−59

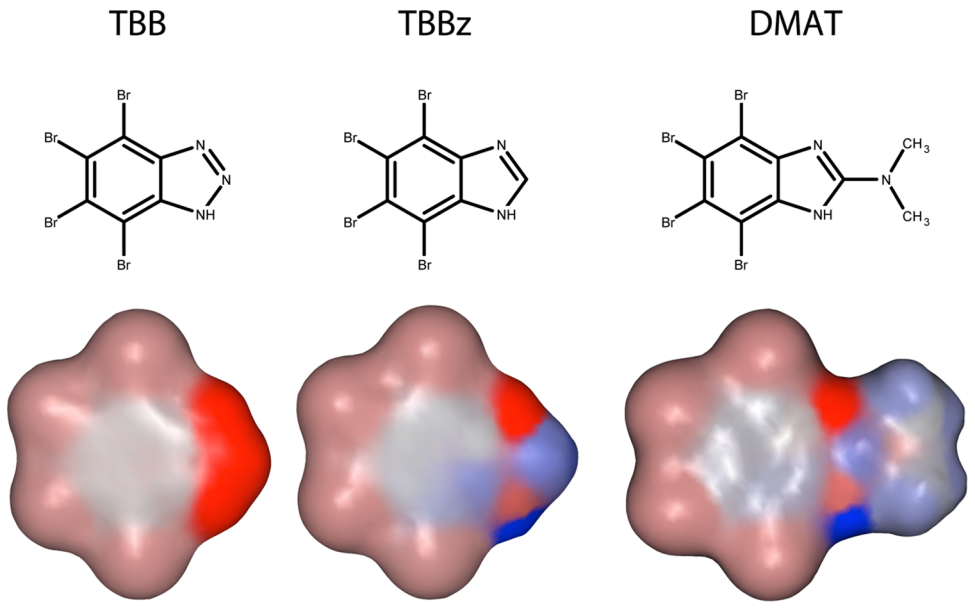

Figure 1. Chemical structure and electrostatic properties of CK2 inhibitors 4,5,6,7-tetrabromobenzotriazole (TBB), 4,5,6,7-tetrabromo-1*H*-benzimidazole (TBBz), and 2-dimethylamino-4,5,6,7-tetrabromo-1*H*-benzimidazole (DMAT). Partial charges were calculated and displayed on the molecular surfaces using Marvin 6.3.1 by ChemAxon (http://www.chemaxon.com).

non-kinase target, NQO2, that eluted from an ATP-Sepharose affinity column when it was washed with TBBz and DMAT but not with a similar concentration of TBB. This corresponded to the rescue experiment in which TBBz and DMAT but not TBB caused cell death and suggests that NQO2 inhibition may contribute to the apoptotic effects of the drugs. Thus, it prompted our investigation of NQO2 inhibition by the three inhibitors.

Historically, NQO2 and related quinone reductases have been characterized as enzymes involved in quinone detoxification. They do so by catalyzing an obligate two-electron transfer to a quinone to produce the relatively stable quinonol, thus preventing non-enzyme-catalyzed single-electron transfer that produces redox active semiquinones.[18] NQO2 is unusual, however, because it uses dihydronicotinamide riboside (NRH) as a reducing coenzyme, rather than NAD(P)H;[19] moreover, in the presence of NRH, NQO2 was found to protect p53 from degradation by the 20S proteasome.[20,21] At the molecular level, reduction of NQO2 and binding of chloroquine (an antimalarial) were shown to induce a conformational change in NQO2, suggesting that NQO2 may function as a flavin redox switch.[22] Therefore, in addition to its role in quinone detoxification, NQO2 appears to have a signaling function, possibly connecting the metabolic status of the cell to p53 levels. While its cellular functions remain to be determined, mice deficient for NQO2 develop skin tumors more frequently than wild-type mice in a chemical carcinogenesis model,[23] indicating that NQO2 plays a role in cell proliferation and/or apoptosis.

In addition to CK2 inhibitors, several chemotherapeutic inhibitors of the Abelson kinase and protein kinase C (PKC) were found to inhibit NQO2 with nanomolar and micromolar affinity, respectively.[24−27] The fact that multiple kinase-directed drugs also inhibit NQO2 raised the question of whether the drug binding site of NQO2 somehow mimics the ATP binding site of kinases. In this study, we performed kinetic and structural analyses to characterize the inhibition of NQO2 by TBB, TBBz, and DMAT. The three inhibitors exhibit different binding profiles with respect to NQO2 that do not correspond to their interactions with CK2.

METHODS

Protein Expression and Purification. Recombinant NQO2 was expressed in *Escherichia coli* and purified as previously described.[28] A critical step in the purification was full reconstitution of the enzyme with the FAD cofactor. When expressed in *E. coli*, recombinant NQO2 typically contains substoichiometric levels of flavin mononucleotide (FMN) and no FAD. A partial denaturation of NQO2 and reconstitution with FAD was incorporated into the purification procedure, leading to full saturation of the enzyme with FAD.[28]

Affinity of Inhibitors by Fluorescence Quenching. To assess direct binding of inhibitors to oxidized NQO2 ($NQO2_{ox}$), fluorescence quenching of FAD was monitored with an excitation wavelength of 350 nm and an emission wavelength of 430 nm. NQO2 (775 or 38.75 nM) was titrated with the indicated concentrations of TBB, TBBz, and DMAT. The binding data were fit to eq 1 to obtain the dissociation constant (K_D) for binding of the inhibitors to $NQO2_{ox}$.

$$(F - F_o)/(F_{max} - F_o) = \left[K_D + I + \mathrm{NQO2} - \sqrt{(K_D + I + \mathrm{NQO2})^2 - 4I \times \mathrm{NQO2}}\right] /(2 \times \mathrm{NQO2}) \quad (1)$$

where NQO2 and I are the final concentrations in the cuvette of the enzyme and inhibitor, respectively, F_o is the initial fluorescence reading in counts per second without an inhibitor, and F is the fluorescence after the addition(s) of TBBz or DMAT. K_D and F_{max} were determined by nonlinear regression using Prism 4.0b (GraphPad Software Inc., San Diego, CA). The data are presented as fractional saturation of NQO2 with an inhibitor $(F - F_o)/(F_{max} - F_o)$.

Enzymatic Assays. Enzyme activity was measured by monitoring the consumption of 1-(3-sulfonatopropyl)-3-

dx.doi.org/10.1021/bi500959t | *Biochemistry* 2015, 54, 47−59

carbamoyl-1,4-dihydropyrimidine (SCDP) (Sigma) coenzyme (a dihydronicotinamide riboside analogue) at an absorbance peak of 360 nm using a Cary 100-Bio spectrophotometer (Varian). The reaction was initiated by addition of NQO2 at a final concentration of 154 pM to a stirring cuvette containing SCDP (10−365 μM) as coenzyme and menadione (0.5−50 μM) (Sigma) as the substrate at 30 °C. The linear portion of the decrease in absorbance was determined using Cary Kinetics Software (Varian) and converted to turnover number (inverse seconds) using the extinction coefficient of SCDP (ε_{360} = 4480 M^{-1} cm^{-1}). Because menadione inhibits the reaction at high concentrations by competing with SCDP for binding to the oxidized enzyme, kinetic data were fit to eq 2 that describes a ping-pong kinetic mechanism with substrate inhibition[29]

$$V_{obs} = \left(V_{max}[SCDP][Md]\right)/\left(K^{app}_{M(SCDP)}[Md] + K_{M(Md)}[SCDP] + [SCDP][Md]\right) \quad (2)$$

where

$$K^{app}_{M(SCDP)} = K_{M(SCDP)}\left[1 + \frac{[Md]}{K_{I(Md)}}\right]$$

where V_{obs} is the observed rate of reaction, V_{max} is the maximal rate, [SCDP] and [Md] are the concentrations of SCDP and menadione, respectively, $K_{M(SCDP)}$ and $K_{M(Md)}$ are the Michaelis constants for substrates SCDP and menadione, respectively, and $K_{I(Md)}$ is the competitive binding constant of menadione. Initial values were obtained from the previous study of NQO2 kinetics using *N*-methyldihydronicotinamide (NeMH) as the coenzyme.[29] Kinetic parameters were fit to the data by nonlinear regression using Igor Pro (Wavemetrics, Portland, OR); the χ^2 values were calculated as

$$\chi^2 = \sum_i \left(\frac{y - y_i}{\sigma_i}\right)^2 \quad (3)$$

where y and y_i are the fitted and measured values, respectively, and σ_i is the estimated standard deviation of the measured value.

Enzyme Inhibition by TBBz and DMAT. To determine the constants for inhibition (K_I values) of NQO2 by TBBz and DMAT, inhibition kinetics were performed using the same techniques that were used for the uninhibited reaction described above. For each inhibitor, kinetic assays were performed either with a constant SCDP concentration of 150 μM and a varying menadione concentration or with a constant menadione concentration of 5 μM and a varying SCDP concentration. Because inhibitors of NQO2 can be competitive against SCDP, menadione, or both, we adapted the kinetic equation to account for both types of inhibition:

$$V_{obs} = \left(V_{max}[SCDP][Md]\right)/\left(K^{app}_{M(SCDP)}[Md] + K^{app}_{M(Md)}[SCDP] + [SCDP][Md]\right) \quad (4)$$

where

$$K^{app}_{M(SCDP)} = K_{M(SCDP)}\left[1 + \frac{[Md]}{K_{I(Md)}} + \frac{[I]}{K_{I(\alpha)}}\right]$$

and

$$K^{app}_{M(Md)} = K_{M(Md)}\left[1 + \frac{[I]}{K_{I(\beta)}}\right]$$

On the basis of eq 2, [I], $K_{I(\alpha)}$, and $K_{I(\beta)}$ were introduced into eq 3, where [I] is the concentration of inhibitor and $K_{I(\alpha)}$ and $K_{I(\beta)}$ are the inhibition constants that modify the "apparent" Michaelis constants $K^{app}_{M(SCDP)}$ and $K^{app}_{M(MD)}$, respectively. That is, $K_{I(\alpha)}$ is the constant that accounts for the change in $K_{M(SCDP)}$ in the presence of inhibitor; hence, it describes the component of inhibition that is competitive against SCDP. $K_{I(\beta)}$ is the constant that accounts for the change in $K_{M(Md)}$ in the presence of inhibitor; hence, it describes the component of inhibition that is competitive against menadione. The kinetic parameters $K_{M(SCDP)}$, $K_{M(Md)}$, and $K_{I(Md)}$ were fixed using values determined for the uninhibited reaction (Table 2), while V_{max}, $K_{I(\alpha)}$, and $K_{I(\beta)}$ were determined by globally fitting data to eq 4 using nonlinear regression (Igor Pro version 6.34A) with the IC_{50} values as initial values.

IC_{50} Measurements. To determine the IC_{50} value of each inhibitor, reactions were initiated by addition of 154 pM NQO2 to a reaction buffer containing 150 μM SCDP and 5 μM menadione with TBB (0.625−640 μM), TBBz (2.5−640 nM), or DMAT (2.5−640 nM). IC_{50} values were then calculated using a dose−response model and represented as relative inhibition.

Crystallization of NQO2. Oxidized NQO2 ($NQO2_{ox}$) was cocrystallized with TBBz or DMAT by hanging drop vapor diffusion against reservoirs containing 0.1 M Hepes (pH 7.5) and 1.3−2.0 M $(NH_4)_2SO_4$. Because TBBz and DMAT are not soluble in mother liquor, TBBz or DMAT (100 μM) was added to a final concentration of 2 mg/mL (77 μM) of NQO2. The NQO2−inhibitor complex was then concentrated 10-fold to 20 mg/mL and used for crystallization.

To obtain a structure of reduced NQO2 in complex with DMAT, reduction of $NQO2_{ox}$−DMAT crystals was performed as previously described.[22] Briefly, $NQO2_{ox}$−DMAT crystals were repeatedly soaked into 1 μL of a reducing soak solution with 0.1 M Hepes (pH 7.5), 2.0 M $(NH_4)_2SO_4$, 10 mM SCDP, and 1 mM DMAT, for 2 min intervals until the crystals were bleached. They were then transferred to a soak without SCDP before briefly being passed through a cryoprotectant solution [2.0 M $(NH_4)_2SO_4$, 0.1 Hepes (pH 7.5), and 20% glycerol] and plunged into liquid nitrogen. To prevent oxidation of NQO2, the entire crystal mounting process from harvesting to cryocooling was performed under an anoxic atmosphere in a glovebag purged with N_2.

X-ray Data Collection, Refinement, and Analysis. Crystallographic data were collected at Canadian Light Source beamline 08ID-1 or from a rotating anode source, processed using MOSFLM,[30] and merged using Scala.[31] The structures were determined by molecular replacement with Protein Data Bank (PDB) entry 1QR2 as a starting model;[32] refinement was conducted using PHENIX.[33] Given the high resolution of the crystallographic data, NCS restraints were not used for any of the refinements. For structures with detectable anomalous scattering ($NQO2_{ox}$−TBBz and $NQO2_{red}$−DMAT), zinc and bromine were refined as anomalous groups. For the oxidized NQO2−DMAT structure, the high resolution of the data allowed for anisotropic refinement of the zinc and bromine atoms. These refinement strategies lowered both R_{work} and R_{free}.

Topology files for TBBz and DMAT were generated using PHENIX.ELBOW.[33] For refinement of the $NQO2_{red}$−DMAT

dx.doi.org/10.1021/bi500959t | *Biochemistry* 2015, 54, 47−59

structure, the FAD topology file was modified to allow bending along the N5−N10 axis of FAD: the planarity restraints incorporating N5 and N10 of the isoalloxazine ring were removed so that it was separated into two planes, one incorporating the pyrimidine ring and the second the benzyl ring. Also, the estimated standard deviations of the bond lengths attached to N5 and N10 were increased 10-fold, and the bond angle and dihedral angle restraints involving N5 and N10 were removed.

To compare FAD bending among the three structures, each structure was refined three times using simulated annealing with the relaxed FAD topology parameters that allow for bending of the isoalloxazine ring. The degree of bending in the isoalloxazine ring was then calculated using principal component analysis incorporating all atoms in each of the two planes, and the angles in each of the three refined structures were averaged. The $NQO2_{ox}$−TBBz, $NQO2_{ox}$−DMAT, and $NQO2_{red}$−DMAT final structures were deposited as PDB entries 4U7G, 4U7H, and 4U7F, respectively.

RESULTS

NQO2 Is a Target of TBB, TBBz, and DMAT. Halogenated benzotriazoles were identified as inhibitors of CK1 and CK2, with 4,5,6,7-tetrabromobenzotriazole (TBB) strongly inhibiting CK2.[7] From this starting point, brominated benzimidazoles, in particular, 4,5,6,7-1*H*-tetrabromobenzimidazole (TBBz) and 2-dimethylamino-4,5,6,7-tetrabromo-1*H*-benzimidazole (DMAT) (Figure 1), that increased selectivity for CK2 were developed.[11,14] DMAT is the most potent of these compounds, exhibiting a 10-fold lower dissociation constant and a 3-fold lower IC_{50} compared to those of TBB and TBBz (Table 1). All three compounds target the ATP binding site of CK2, and on this basis, it is not surprising that they are also active against other kinases.[15] On the other hand, it was surprising that both TBBz and DMAT were identified as interactors with NQO2, which neither is a kinase nor has a known ATP binding site.[17] However, NQO2 does bind other kinase inhibitors,[24,27] raising the possibility that its active site mimics a kinase binding site. Our goal in this study was to characterize the binding and inhibition of NQO2 by these three compounds and compare their activities against NQO2 with those against CK2.

Table 1. Binding Affinity and Inhibition of TBB, TBBz, and DMAT with Respect to CK2 and NQO2

	K_D		IC_{50}	
inhibitor	CK2[a]	NQO2[b]	CK2[a]	NQO2[c]
TBB	400 nM	7.11 ± 0.04 μM	500 nM	12.8 ± 2 μM
TBBz	700 nM	18.1 ± 0.4 nM	500 nM	79.4 ± 12 nM
DMAT	40 nM	36.4 ± 1.7 nM	140 nM	484 ± 80 nM

[a] K_D and IC_{50} values for CK2 were reported previously.[12,36] [b] The dissociation constants for oxidized NQO2 were determined by fluorescence titrations; values are means ± the standard deviation for three independent titrations. [c] IC_{50} values for NQO2 were determined by an *in vitro* assay with 150 μM SCDP and 5 μM menadione and varying concentrations of inhibitors. Kinetic data were fit to a sigmoidal response curve (Figure 2B); values are the estimated IC_{50} ± the range of the 95% confidence interval.

TBB, TBBz, and DMAT are planar aromatic compounds and as such are expected to bind to NQO2 by stacking onto the isoalloxazine ring of FAD. On this basis, fluorescence titrations were used to directly measure binding affinities for oxidized NQO2. Both TBBz and DMAT bound tightly to NQO2, with K_D values of 18 and 36 nM, respectively, while TBB bound much more weakly with a K_D of 7.1 μM (Table 1 and Figure 2A). To characterize the ability of these compounds to inhibit

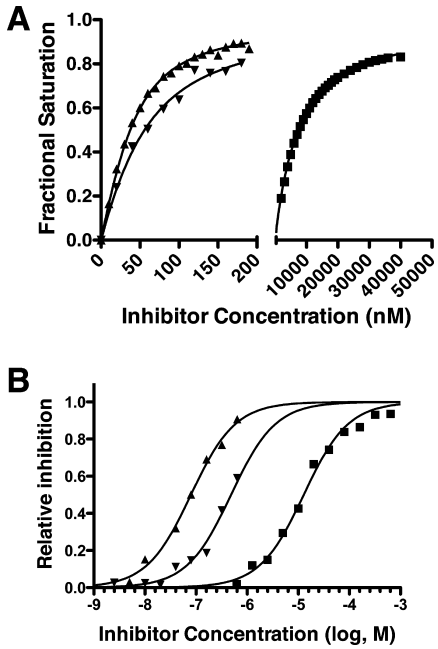

Figure 2. Binding and inhibition of NQO2 by TBBz, DMAT, and TBB. (A) Representative data for binding of TBBz (▲), DMAT (▼), and TBB (■) to oxidized NQO2. Binding was characterized by fluorescence titrations of the inhibitors against oxidized NQO2 at a concentration of 38.75 nM (TBBz and DMAT) or 775 nM (TBB). The stirred sample was monitored at an excitation wavelength of 350 nm and an emission wavelength of 430 nm. The solid curves represent the binding isotherms, which were determined by nonlinear regression as outlined in Methods; the dissociation constants for the inhibitors are listed in Table 1. (B) Inhibition of steady-state catalysis by TBBz (▲), DMAT (▼), and TBB (■). Reactions were initiated with the addition of 154 pM NQO2 to 150 μM SCDP and 5 μM menadione and varying concentrations of the inhibitors; IC_{50} values were calculated from these data and are listed in Table 1.

NQO2's enzymatic activity, IC_{50} values were determined using an *in vitro* assay (Figure 2B). NQO2 operates by a ping-pong catalytic mechanism: the first step is reduction of the FAD isoalloxazine ring by dihydronicotinamide riboside (NRH), followed by dissociation of the oxidized nicotinamide and binding of a quinone substrate. For the assay, a commercially available NRH analogue, 1-(3-sulfonatopropyl)-3-carbamoyl-1,4-dihydropyrimidine (SCDP), which exhibits a change in absorbance at 360 nm upon oxidation by NQO2, was used along with menadione as the quinone substrate. All three compounds inhibited the enzymatic activity of NQO2. The IC_{50} values were all higher than the dissociation constants, but the difference depended on the compound (Table 1). That is, the IC_{50} value for DMAT was >12-fold higher than its K_D, while the IC_{50} value for TBBz was 4-fold higher; for the relatively weak binding inhibitor, TBB, the IC_{50} was only slightly greater than the K_D (Table 1). This indicates that the compounds are inhibiting NQO2 through somewhat different mechanisms.

dx.doi.org/10.1021/bi500959t | *Biochemistry* 2015, 54, 47−59

The activity profiles of TBB, TBBz, and DMAT against NQO2 are different from those against CK2. First, both TBB and TBBz bind to CK2 with roughly equal affinity (K_D values of 400 and 700 nM, respectively), whereas with NQO2, the binding of TBB is almost 3 orders of magnitude weaker than that of TBBz. Second, a comparison of DMAT and TBBz shows that DMAT binds to CK2 with an affinity more than 1 order of magnitude greater than that of TBBz, whereas binding of DMAT to NQO2 is slightly weaker than that of TBBz (Table 1). Finally, the large differences between K_D and IC_{50} values observed for NQO2 (particularly in the case of DMAT) were not observed for CK2; instead, for CK2, the IC_{50} and K_D values for TBB and TBBz were almost equal, and the IC_{50} for DMAT was only 3-fold greater than the K_D. On the basis of these binding and inhibition data, the properties of the NQO2 binding site do not fully mimic the properties of the CK2 ATP binding site. To improve our understanding of the interactions between NQO2 and the nanomolar inhibitors TBBz and DMAT, we performed a more detailed kinetic analysis to determine the mode of enzymatic inhibition.

Kinetic Analysis of Inhibition of NQO2 by TBBz and DMAT. The ping-pong catalytic mechanism of NQO2 means that the active site cycles through an oxidized state and a reduced state for each catalytic turnover. In this study, the steady-state kinetic parameters of the uninhibited reaction were determined using the NRH analogue SCDP as the coenzyme and menadione as the substrate. Because previous studies have shown that menadione acts as a competitive inhibitor toward SCDP,[29] substrate inhibition by menadione was incorporated into the kinetic model (eq 2, Methods). Consistent with previous results, our kinetic data (Figure 3) confirm that the

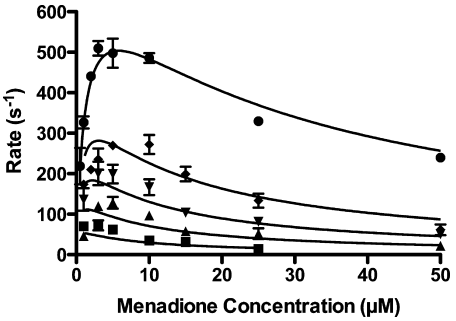

Figure 3. Steady-state ping-pong kinetics of NQO2 with substrate inhibition. Steady-state kinetic analysis was performed to obtain the kinetic parameters listed in Table 2. Initial concentrations of SCDP were 10 (■), 25 (▲), 50 (▼), 100 (◆), and 365 (●) μM, and concentrations of menadione varied as indicated. Data points are measured rates, and solid curves represent the nonlinear regression fits derived from globally fitting all data to eq 1 (Methods) that describes a ping-pong kinetic mechanism with substrate inhibition by menadione. The χ^2 value for the global fit was 7.4×10^4.

binding of menadione to oxidized NQO2 [$K_{I(Md)}$] is similar to the Michaelis constant of menadione [$K_{M(Md)}$ (Table 2)]. Thus, menadione exhibits limited discrimination between the two redox states of NQO2.

An inhibitor of NQO2 can be competitive toward the SCDP coenzyme and/or the quinone substrate depending on whether the inhibitor binds preferentially to the oxidized or reduced form of NQO2. We used eq 4 (Methods) to account for the competitive inhibition model. In this model, each inhibitor is expected to compete with SCDP, menadione, or both, and the

Table 2. Steady-State Kinetic Parameters of Quinone Reductase 2

parameter[a]	value
k_{cat}	981 ± 90.4 s^{-1}
$K_{M(SCDP)}$	142 ± 23.2 μM
$K_{M(menadione)}$	1.62 ± 0.31 μM
$K_{I(menadione)}$	8.07 ± 1.48 μM

[a]Calculated by globally fitting rate data to eq 2, as described in Methods.

inhibition constants $K_{I(\alpha)}$ and $K_{I(\beta)}$ describe the degree to which the presence of the inhibitor alters the apparent Michaelis constants for the reaction. Another way of viewing the $K_{I(\alpha)}$ or $K_{I(\beta)}$ constants is that their relative values should indicate the preference of the inhibitor for either the oxidized or reduced form of NQO2, respectively. Global fitting of the rate data (Figure 4) to eq 4 yielded values of $K_{I(\alpha)}$ and $K_{I(\beta)}$ for TBBz and DMAT as well as k_{cat} values (Table 3). Thus, the inhibition constant of TBBz toward SCDP ($K_{I(\alpha)}$ = 19.6 ± 2.9 nM) is very close to the binding affinity of TBBz for oxidized NQO2 (K_d = 18.1 ± 0.4 nM). The high value and very high standard error for the inhibition constant of TBBz toward the quinone substrate, menadione ($K_{I(\beta)}$ = 865 ± 3790 nM), indicate that the interaction of TBBz with the oxidized form of NQO2 is sufficient to completely account for TBBz-mediated inhibition, and therefore, binding to the reduced form cannot be assessed using steady-state kinetics. The situation for DMAT is more complicated: the inhibition constant of DMAT toward SCDP ($K_{I(\alpha)}$ = 121 ± 20 nM) is 3-fold higher than its affinity for oxidized NQO2 (K_d = 36.4 ± 1.7 nM). Furthermore, we find that the inhibition constant of DMAT toward menadione ($K_{I(\beta)}$ = 302 ± 131 nM) is similar to its inhibition constant against SCDP. This indicates that DMAT is binding to both oxidized and reduced NQO2; it exhibits relatively poor discrimination between the two. This was surprising but not unprecedented as the substrate menadione also shows poor discrimination between the two redox states of NQO2; however, DMAT is the first inhibitor shown to exhibit similar affinity for both redox states of NQO2.

Structures of Oxidized NQO2 with TBBz and DMAT. Crystal structures of NQO2−inhibitor complexes were used to determine the structural basis for binding of TBBz and DMAT to oxidized NQO2. Cocrystallization of NQO2 and TBBz yielded crystals that diffracted to 1.86 Å; the structure was determined by molecular replacement and refined to an R_{free} value of 0.2288 (Table 4). Crystals of NQO2 contain a dimer in the asymmetric unit, and TBBz was modeled in two orientations in both active sites of the NQO2 dimer. Because TBBz has four bromine atoms that contribute to anomalous scattering, the first orientation of TBBz was modeled using an anomalous difference map that indicated four prominent peaks (two peaks at 5−6σ and two peaks at 4σ) in the active site of NQO2 (Figure 5A). In the first orientation, the tetrabromobenzene makes π-stacking interactions with the FAD isoalloxazine ring and the phenyl ring of F178. Bromine atoms 4 and 5 of TBBz make halogen bonds[34] to the backbone carbonyl of G174 and to the carboxyamide of N161. The benzimidazole nitrogen makes a π-hydrogen bond[35] with the benzene ring of the W105 indole side chain. During the refinement, inconsistencies in the relative values for the atomic displacement parameters (ADPs) within the imidazole ring of TBBz suggested that TBBz was binding in an alternative

dx.doi.org/10.1021/bi500959t | Biochemistry 2015, 54, 47−59

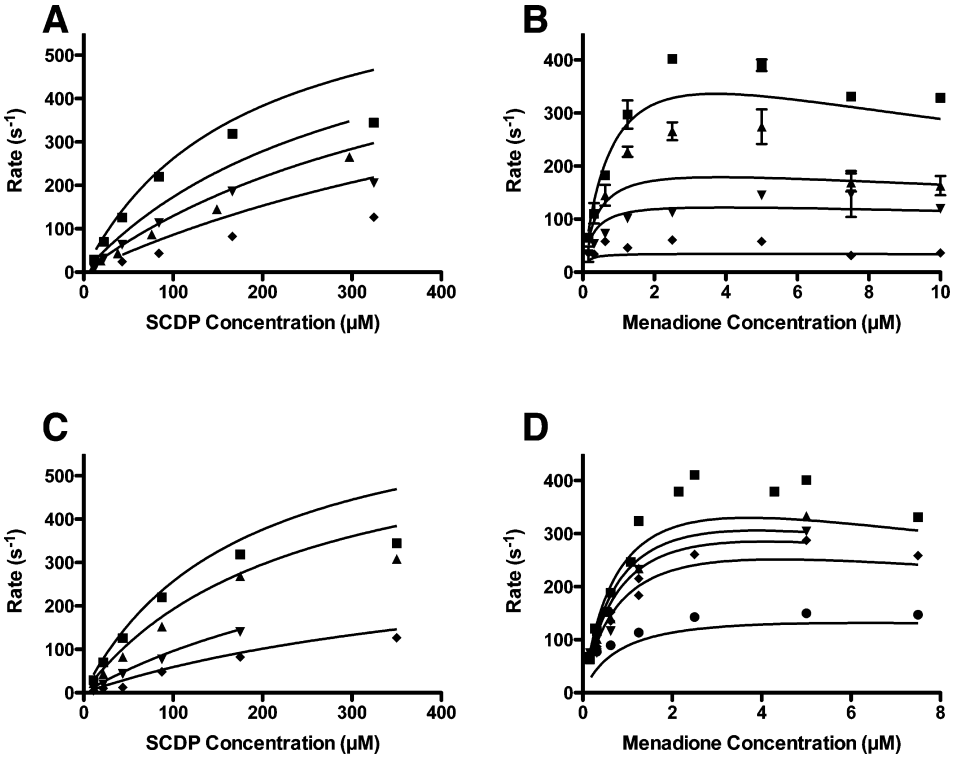

Figure 4. Kinetic analysis of NQO2 inhibition by TBBz and DMAT. Steady-state rate measurements of NQO2-catalyzed reduction of menadione were taken in the presence of TBBz (A and B) or DMAT (C and D) to obtain the values for $K_{I(\alpha)}$, $K_{I(\beta)}$, and k_{cat} listed in Table 3. In panels A and C, assays included a constant menadione concentration of 5 μM, while in panels B and D, assays included a constant SCDP concentration of 150 μM. The concentrations of TBBz were 0 (■), 50 (▲), 100 (▼), and 500 (◆) nM (A) and 0 (■), 25 (▲), 50 (▼), and 100 (◆) nM (B). The concentrations of DMAT were 0 (■), 100 (▲), 500 (▼), and 1000 (◆) nM (C) and 0 (■), 25 (▲), 50 (▼), 100 (◆), and 500 (●) nM (D). The solid curves in the panels represent global fits to all of the data in panels A and B [to obtain $K_{I(\alpha)}$, $K_{I(\beta)}$, and k_{cat} for inhibition by TBBz] or panels C and D [to obtain $K_{I(\alpha)}$, $K_{I(\beta)}$, and k_{cat} for inhibition by DMAT]. The χ^2 value for the global fit to TBBz-inhibited NQO2 (A and B) was 1.4×10^5, while that for the DMAT-inhibited NQO2 (C and D) was 4.6×10^4.

Table 3. Inhibition of NQO2 by TBBz and DMAT

inhibitor	$K_{I(\alpha)}$[a] (nM)	$K_{I(\beta)}$[b] (nM)	k_{cat} (s^{-1})
TBBz[c]	19.6 ± 2.9	865 ± 3790	949.8 ± 34.5
DMAT[d]	121 ± 20	302 ± 131.0	884.0 ± 19.2

[a]$K_{I(\alpha)}$ is the component of the inhibition that is competitive against SCDP. [b]$K_{I(\beta)}$ is the component of the inhibition that is competitive against menadione. [c]The parameters (with standard errors) were calculated by globally fitting the rate data illustrated in panels A and B of Figure 4. [d]The parameters (with standard errors) were calculated by globally fitting the rate data illustrated in panels C and D of Figure 4.

orientation (Figure 5B). The second orientation of TBBz is related by a 60° rotation around the benzene ring that places a bromine atom in the position of one of the benzimidazole nitrogens. Refinement of the structure with the two TBBz orientations yielded consistent values for the ADPs. As a result of the rotation, the halogen bonds to G174 and N161 are maintained but are made with bromines 5 and 6 rather than bromines 4 and 5 as in the first orientation. In addition, the π-hydrogen bond to the W105 indole is replaced with an interaction between bromine 4 and the W105 side chain. Thus, both orientations of TBBz involve similar interactions with NQO2.

Oxidized NQO2 was also cocrystallized with DMAT. Data from an $NQO2_{ox}$–DMAT crystal were collected to 1.5 Å, and the structure was refined to an R_{free} value of 0.2023 (Table 4). Because these data were collected from a synchrotron source at a wavelength farther from the bromine edge, the anomalous signal for bromine was weaker. Nonetheless, DMAT was modeled in two orientations by anchoring the bromines to anomalous scattering peaks (Figure 5C,D). Like the $NQO2_{ox}$–TBBz complex, DMAT makes π-stacking interactions with the FAD isoalloxazine ring and the phenyl ring of F178. The first orientation of DMAT is similar to that of TBBz, in which the inhibitor makes two halogen bonds to the backbone carbonyl of G174 and the carboxyamide of N161; however, the dimethylamine substituent of DMAT prevents the benzimidazole nitrogen from making a π-hydrogen bond with W105. The alternate orientation of DMAT (Figure 5D) is rotated 60° clockwise and binds in an orientation almost identical to that of TBBz (Figure 5B). As one might anticipate from their structures, TBBz and DMAT show very similar modes of binding to the NQO2 active site. The fact that the dimethylamine moiety of DMAT prevents it from binding optimally in the preferred mode explains its slightly lower affinity for NQO2 (a K_D of 36 nM compared to a K_D of 18 nM for TBBz).

Binding of DMAT to Reduced NQO2. Our kinetic analysis indicated that DMAT binds with a similar affinity to the reduced and oxidized forms of NQO2. To elucidate the mode of binding of DMAT to reduced NQO2, crystals of oxidized NQO2 in complex with DMAT ($NQO2_{ox}$–DMAT) were reduced in a soaking solution containing SCDP. A data set from a crystal of the $NQO2_{red}$–DMAT complex was collected to 1.90 Å and the structure refined to an R_{free} value of 0.2268 (Table 4). It was clear that reduction of the FAD coenzyme had

dx.doi.org/10.1021/bi500959t | Biochemistry 2015, 54, 47–59

Table 4. Crystallographic Data Collection and Refinement Statistics

	oxidized NQO2		reduced NQO2
	TBBz	DMAT	DMAT
wavelength (Å)	1.54	1.03	1.54
space group	$P2_12_12_1$	$P2_12_12_1$	$P2_12_12_1$
unit cell dimensions (Å)	56.24, 83.17, 106.65	56.25, 83.01, 106.48	56.12, 83.14, 106.46
resolution (Å)	18.18−1.91	30.02−1.45	17.99−1.73
R_{sym} [a]	0.098 (0.57)	0.06 (0.43)	0.073 (0.66)
$I/\sigma(I)$ [a]	7.5 (2.0)	9.7 (1.7)	14.8 (2.6)
completeness [a]	92.8 (57.3)	96.0 (74.5)	89.9 (74.5)
redundancy	4.4	4.6	6.2
no. of unique reflections	36697	85781	47314
R_{work}/R_{free}	0.1745/0.2288	0.1843/0.1958	0.1840/0.2254
Ramachandran plot [b] (%)			
most favored	90.2	91.7	90.7
additionally allowed	9.3	7.8	8.8
generously allowed	0.5	0.5	0.5
disallowed	0	0	0
root-mean-square deviation			
bond lengths (Å)	0.009	0.010	0.009
bond angles (deg)	1.150	1.353	1.128
dihedral angles (deg)	14.665	14.702	14.238
mean ADP value (Å^2)			
protein			
all atoms	20.990	21.913	23.698
main chain	20.084	20.285	22.608
side chain	21.913	23.282	24.809
solvent			
water	27.553	31.850	26.960
FAD	22.305	22.682	25.113
inhibitor	26.988	46.165	37.759

[a]Values in parentheses refer to the highest-resolution shell. [b]Ramachandran plot statistics were calculated using PROCHECK.[65]

a major effect on binding of DMAT: it was less deeply buried in $NQO2_{red}$ than in $NQO2_{ox}$, and the space made available was filled with water molecules that mediate interactions between DMAT and reduced NQO2. As with the oxidized NQO2−DMAT complex, DMAT bound to the reduced enzyme in two orientations: this was clear from the presence of three strong anomalous scattering peaks representing the common positions of the bromine atoms in the two orientations (Figure 5E,F). Two of the bromines interact with three water molecules (numbers 32, 16, and 85) that in turn are hydrogen-bonded to the backbone carbonyl of G174 and the carboxyamide of N161. The third common bromine atom makes a π-halogen bond to the W105 indole group. The less deeply buried position of DMAT in the reduced NQO2 structure means that it no longer makes π-stacking interactions with F178, and the area in contact with the isoalloxazine ring is also reduced.

Structural Changes in FAD in the $NQO2_{red}$−DMAT Complex. The reduction of the planar isoalloxazine ring of FAD leads to a "butterfly bend" along the N5−N10 axis.[36] On this basis, refinement of the $NQO2_{red}$−DMAT structure was conducted using a modified stereochemical restraint set for FAD, in which planar restraints and associated bond and angle restraints around N5 and N10 were removed. The final refined structure indicated butterfly bend angles of 3.0° and 5.4° for the isoalloxazine ring systems in chains A and B, respectively. To validate that the small change in the FAD isoalloxazine structure was due to reduction of the FAD, and not simply removal of stereochemical restraints, the refined NQO2 structures were further subjected to simulated annealing refinement against data from both oxidized and reduced crystals (Table 5). In the absence of stereochemical restraints around N5 and N10, the isoalloxazine ring of $NQO2_{ox}$ in complex with TBBz refined to 1.8° and 2.4° for each FAD coenzyme; for $NQO2_{ox}$ in complex with DMAT, the bend was 2.7° and 2.4° for each FAD coenzyme. Thus, FAD is bent approximately 2° upon reduction and binding of DMAT.

DISCUSSION

TBB, TBBz, and DMAT are ATP-competitive inhibitors of CK2 that reduce the level of autophosphorylation of CK2β by CK2α and CK2α'. The three inhibitors induce apoptosis in HeLa, Jurkat, and HL-60 cells[10,14,17,37] ostensibly by preventing CK2 function to promote cell survival over apoptosis.[3,38,39] However, both TBBz and DMAT, but not TBB, were potent inducers of apoptosis in cells expressing an inhibitor-resistant CK2. Furthermore, in cells expressing wild-type CK2, both TBBz and DMAT are more potent inducers of apoptosis than TBB.[10,14,17,37] On this basis, interactions of TBBz and DMAT with molecule(s) other than CK2 appear to contribute to their induction of apoptosis. Through a proteomics screen, NQO2 was identified as a target of TBBz and DMAT, but not TBB. In the study presented here, we have shown that both TBBz and DMAT bind to and inhibit NQO2 at nanomolar concentrations, whereas the interaction between NQO2 and TBB is much weaker. The interactions of TBB, TBBz, and DMAT with NQO2 therefore correlate with their apoptotic effects in cells transformed with inhibitor-resistant CK2.[17] Because several other kinase inhibitors also bind NQO2,[24,25,27,40] we sought to

dx.doi.org/10.1021/bi500959t | Biochemistry 2015, 54, 47−59

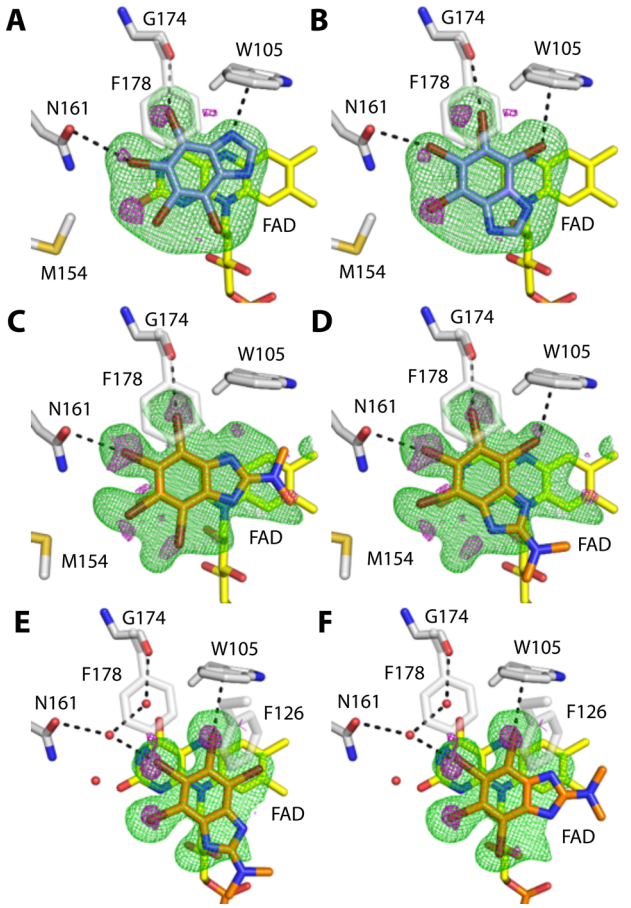

Figure 5. Binding of TBBz and DMAT to oxidized and reduced NQO2. Complexes between oxidized NQO2 and TBBz or DMAT (A–D) show the inhibitors are sandwiched between the isoalloxazine ring of FAD (yellow) and F178 (above the plane of the inhibitor). (A) In one orientation, TBBz makes two halogen bonds and a π-hydrogen bond to N161, G174, and W105, respectively. (B) In its second orientation, TBBz is rotated 60° to make three halogen bonds with N161, G174, and W105. (C) DMAT makes two halogen bonds to N161 and G174 in one orientation, but the presence of the dimethylamine group hinders the imidazole nitrogen from π-hydrogen bonding with W105. (D) In the second orientation, DMAT makes three halogen bonds with N161, G174, and W105, similar to what was observed for TBBz. In the structure of reduced NQO2 (E and F), DMAT occupies a more peripheral position, makes fewer π-stacking interaction with FAD, no longer contacts F178, and instead makes somewhat stronger hydrophobic contact with F126. (E) In one orientation of DMAT, bromine 6 makes a halogen bond to a water molecule, which is in turn bonded to N161, while bromine 5 makes a halogen bond to W105. (F) In the second orientation with reduced NQO2, DMAT is rotated 60° and the same halogen bonds are mediated by bromines 4 and 5. The electron density maps represent the $F_o - F_c$ (green mesh) and anomalous (magenta mesh) differences calculated after simulated annealing with the inhibitors omitted from the structure; all electron density maps were contoured at 3σ around the inhibitors. In all three structures, the inhibitor binding orientations are the same for both subunits (the A and B chains) of the NQO2 dimer that constitutes the asymmetric unit of the crystal.

understand the structural basis for the interaction between NQO2 and TBBz or DMAT. In particular, we wanted to determine how similar the active site of NQO2 was to the ATP binding site of CK2 and other kinases.

While TBB, TBBz, and DMAT all bind CK2 with nanomolar affinity[11,14,41] (Table 1), the affinity of TBB for oxidized NQO2

Table 5. Conformational Changes in the Isoalloxazine Ring upon Reduction

NQO2	inhibitor	subunit	N5–N10 bend[a]
oxidized	TBBz	A	1.81 ± 0.06
		B	2.44 ± 0.04
		average	2.13
	DMAT	A	2.74 ± 0.01
		B	2.39 ± 0.06
		average	2.57
reduced	DMAT	A	2.95 ± 0.11
		B	5.37 ± 0.23
		average	4.16

[a]Both oxidized and reduced structures were subjected to three separate rounds of simulated annealing refinement in the absence of planar restraints for the N5–N10 axis and angle restraints for the C4X–N5–C5X/C10–N10–C9A angles. The butterfly bend along the N5–N10 axis was calculated using the atomic positions of the dimethylbenzene and pyrimidine "wings" and principle component analysis to find the angle between the two best-fit planes.

is 3 orders of magnitude lower than that of TBBz and DMAT (Table 1). Similarly, the IC_{50} values of TBB, TBBz, and DMAT for inhibition of NQO2 are dramatically different (Table 1), with TBB exhibiting much weaker inhibition of NQO2, consistent with its relatively low binding affinity. The difference in binding affinities between TBB and TBBz/DMAT can be explained by the charge of the inhibitors (Figure 1). The triazole function of TBB has an estimated pK_a of 5 and is expected to be anionic at physiological pH, whereas the imidazole functions of TBBz and DMAT have pK_a values of approximately 9 and will therefore be neutral at physiological pH.[37] In CK2, the negatively charged triazole portion of TBB interacts with a region of positive electrostatic potential (Figure 6A,B).[6,42] In the case of oxidized NQO2, the surface of the active site has a negative electrostatic potential that precludes high-affinity interactions with anionic TBB (Figure 6C). Thus, differences in the electrostatic potential of the active sites of NQO2 and CK2 explain why TBB binds with a relatively low affinity to the NQO2 active site.

DMAT and TBBz bind with a similar high affinity to oxidized NQO2, and our structural analysis shows that they bind in a similar manner, stacking on top of the isoalloxazine ring of FAD with the bromine atoms making halogen bonds to nearby carbonyl groups as well as the indole side chain of W105 (Figure 5). Both TBBz and DMAT bind in two orientations. For TBBz, the preferred orientation is one in which two bromine atoms and one of the imidazole nitrogens make bonds with two carbonyl groups and W105, respectively (Figure 5A). The small difference in affinity between TBBz and DMAT is likely due to the inability of DMAT to fully adopt the preferred conformation (Figure 5A) because of a steric clash between its dimethylamine function and the indole side chain of W105 (Figure 5C). Structures of CK2 in complex with TBBz and DMAT show that the two inhibitors bind to the CK2 active site in an identical manner (PDB entries 1ZOE and 2OXY, respectively).[42,43] In CK2, the two drugs are sandwiched between hydrophobic residues and two of the bromine atoms make halogen bonds with backbone carbonyl groups of E114 and V116 (Figure 6B). In the case of CK2, DMAT binds with 10-fold greater affinity than TBBz because of additional favorable interactions mediated by the dimethylamine group.

dx.doi.org/10.1021/bi500959t | Biochemistry 2015, 54, 47–59

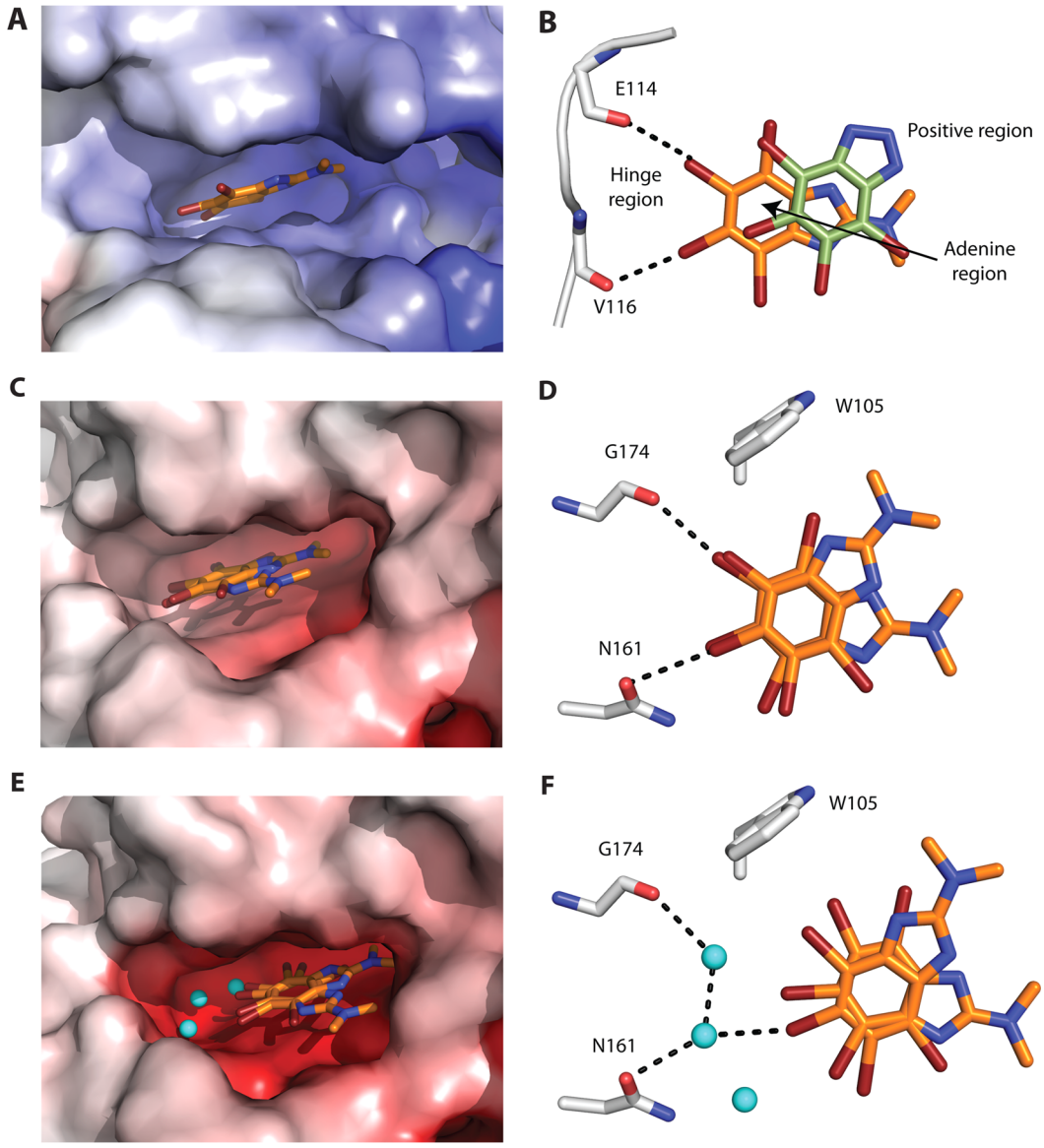

Figure 6. Binding of DMAT to CK2, oxidized NQO2, and reduced NQO2. (A) The molecular surface of the CK2 active site is shown with bound DMAT (PDB entry 1ZOE)[43] and colored according to electrostatic potential. (B) Details of interactions between DMAT (orange carbons) and the CK2 active site. Note that TBBz (not displayed) binds in exactly the same manner as DMAT.[42] The position of CK2-bound TBB (green carbons, PDB entry 1J91)[62] is also shown: the negative charge of the triazole moiety (Figure 1) causes a shift toward a more positively charged region in the CK2 active site.[42] (C) Molecular surface of the active site in oxidized NQO2 with bound DMAT in two orientations. (D) Details of the binding of DMAT to oxidized NQO2. (E) Molecular surface of reduced NQO2 with bound DMAT in two orientations, including three water molecules (cyan) that are present in the reduced, but not the oxidized, structure. (F) Details of the binding of DMAT to reduced NQO2. Electrostatic potentials were calculated using APBS,[63] and partial charges were calculated using PDB entry 2PQR.[64] In the case of oxidized FAD, the sum of the partial charges in the isoalloxazine ring yielded an overall charge of −0.2; for reduced FAD, an additional full charge was added and distributed roughly evenly between the N1 and O2 atoms. The figures were made in PyMol (version 1.7.0.5, Schrödinger, LLC), and the color limits for the electrostatic surfaces were set to −12 *kT* (red) to 12 *kT* (blue) for all three structures.

In summary, the NQO2 active site appears to mimic the adenine binding site of CK2 in the sense that it provides a hydrophobic crevice that can accommodate planar aromatic molecules, and there are two carbonyl groups that are well-placed to mediate charge interactions with the bromine atoms of these inhibitors in a manner similar to that observed in CK2. On the other hand, NQO2 provides an environment that allows both TBBz and DMAT to bind in alternate orientations, whereas binding to CK2 is limited to a single orientation. Furthermore, the presence of the dimethylamine group on DMAT favors binding to CK2 but disfavors binding to NQO2. These observations, in addition to the striking differences in the electrostatic potential in the two active sites, indicate that the binding of TBBz and DMAT to NQO2 is adventitious and on the whole the NQO2 active site is not a good mimic of the CK2 active site.

Another major difference between the active sites of NQO2 and CK2 is that the NQO2 active site can exist in either an oxidized or reduced form. The origin of the change in oxidation state is the isoalloxazine ring of FAD: upon interaction with a reduced nicotinamide coenzyme (NRH or SCDP), two electrons are transferred onto the isoalloxazine ring of FAD.[44] Upon reduction, the N5 atom is protonated and its orbital changes from planar sp^2 to trigonal pyramidal sp^3 hybridization.

dx.doi.org/10.1021/bi500959t | *Biochemistry* 2015, 54, 47−59

These changes allow it to donate a hydrogen bond, and the change in orbital hybridization also disrupts the planarity of the isoalloxazine ring, leading to a small butterfly bend. Thus, reduction of FAD leads to a relatively minor structural change in the isoalloxazine ring but more importantly imparts a negative charge that will be largely centered around N1 and O2 of the isoalloxazine ring. Our crystallographic study indicates that reduction of the isoalloxazine ring completely changes the mode of binding of DMAT: it binds in a more peripheral location, and the interactions of the bromine atoms with the carbonyl groups are mediated through intervening water molecules.

Compounds that bind with high affinity to only one form of NQO2, either oxidized or reduced, exhibit predictable effects on the steady-state kinetics of the system. Thus, TBBz binds with high affinity to oxidized NQO2 and competes with SCDP, resulting in significant changes in the apparent Michaelis constant for SCDP; furthermore, the inhibition constant against SCDP is close to its dissociation constant, as expected. This does not mean that TBBz completely fails to bind to reduced NQO2; in fact, given the similarity between TBBz and DMAT, it is likely that TBBz binds to the reduced form of NQO2 in a manner similar to that observed for DMAT. However, because the affinity of the interaction between TBBz and reduced NQO2 is relatively weak compared to binding of TBBz to oxidized NQO2, the inhibition observed in the steady-state kinetic analysis is due almost entirely to its binding to oxidized NQO2, and therefore, TBBz has little impact on the Michaelis constant for menadione.

The situation appears to be more complicated for an inhibitor such as DMAT that binds with similar affinities to both oxidized and reduced NQO2. The lower affinity of DMAT for oxidized NQO2 made the interaction between DMAT and reduced NQO2 apparent in our steady-state kinetic analysis, where the presence of DMAT had a significant effect on the Michaelis constants for both SCDP and menadione. In this case, changes in both Michaelis constants were used to calculate inhibition constants (K_I values) of 121 nM against SCDP and 302 nM against menadione, both of which are significantly higher than the dissociation constant (36 nM) for binding of DMAT to oxidized NQO2. This is a confusing result because the inhibition constant is expected to represent a dissociation constant for the inhibitor. The relatively high K_I values for DMAT are in line with the high IC_{50} for DMAT, which is 6-fold higher than the IC_{50} for TBBz, despite the fact that DMAT binds to oxidized NQO2 with a K_D that is only twice as high as that of TBBz. It seems as though the ability of DMAT to bind with similar affinities to both the oxidized and reduced forms of NQO2 actually weakens its ability to inhibit NQO2-mediated catalysis. Although we can only speculate about the molecular origins of this effect, it highlights the complicated nature of NQO2 and the fact that binding interactions may have unpredictable effects on catalysis and, by extension, *in vivo* function.

Inhibition of NQO2 by Other Kinase Inhibitors. Interestingly, NQO2 was also found to be the only non-kinase target of two Abl kinase inhibitors as well as protein kinase C bisindolylmaleimide inhibitors.[24,25,27] Specifically, the cancer wonder drug imatinib and its second-generation derivative, nilotinib, were found to bind and inhibit NQO2. Structural investigation showed that rings A and B of imatinib that occupy the ATP binding site of the Abelson kinase were also found to occupy the active site of NQO2.[26] While imatinib does not inhibit CK2[45] and CK2 inhibitors do not inhibit the BCR-ABL kinase,[15] both were found to interact with the non-kinase target NQO2.[17,25] Therefore, there are several classes of kinase inhibitors that bind NQO2 fortuitously, and the specific cellular effects of these kinase inhibitors may be due in part to their interaction with NQO2.

One of the cellular functions of NQO2 may be the detoxification of quinones by two-electron reduction; however, the natural substrates have not been identified, and it is not obvious why NQO2 would have evolved a preference for NRH over NAD(P)H to fulfill a detoxification function. A second possible function for NQO2 may involve cellular signaling in response to changes in metabolic and/or redox status. In particular, NQO2 was shown to stabilize p53 from 20S proteasomal degradation in the presence of NRH.[20,21] While the canonical degradation pathway of p53 is ubiquitin-dependent and uses the 26S proteasome, degradation by the 20S proteasome is ubiquitin-independent and is modulated by quinone reductase 1 (NQO1) and NQO2.[20,21,46] Interestingly, NQO1, the "sister enzyme" of NQO2, uses NAD(P)H as a coenzyme and is specific for a different set of inhibitors. Given their difference in coenzyme specificity, NQO1 and NQO2 may be regulating p53 stability in response to changes in the cellular redox state, as reflected in the levels of NAD(P)H and NRH, but this remains a matter of speculation. Strikingly, numerous NQO2 inhibitors such as melatonin, resveratrol, chloroquine, imatinib, 9-aminoacridine, and quinacrine have been shown to induce p53-dependent apoptosis.[47−51] Melatonin and resveratrol both induce p53 phosphorylation at serine 15, which is essential to the transactivation of p53-induced apoptotic genes;[47,50] chloroquine, 9-aminoacridine, and quinacrine, on the other hand, increase p53 levels without phosphorylation at serine 15, which is thought to lead to transcription-independent apoptosis modulated by p53.[48,51,52] The fact that NQO2 binds all of these bioactive compounds is remarkable, but a contribution from NQO2 to the cellular effects of these compounds has yet to be demonstrated.

The cellular roles of NQO2 are still very much a matter of debate. In this regard, the cellular effects of two high-affinity (nanomolar) inhibitors of NQO2 have been investigated. S29434 was developed by the French pharmaceutical company Servier as a compound that inhibits the third melatonin binding site (MT3), which is NQO2, without inhibition of the two other melatonin binding sites, both of which are G-protein-coupled receptors.[53,54] S29434 prevents generation of reactive oxygen species *in vitro* and *in vivo*, and it prevents paraquat-induced toxicity to cell lines in a ROS-dependent manner.[55,56] Similarly, NQO2 knockout mice were resistant to menadione-induced toxicity,[57] which likely occurs through oxidative stress resulting from NQO2-mediated metabolism of menadione. Therefore, inhibitors of NQO2 can prevent cell death caused by compounds that are toxic when they are metabolized by NQO2; however, inhibition of NQO2 appears to have little effect on cells in the absence of these toxic compounds.

A second series of inhibitors, based on an imidazoacridin-6-one core, was identified through a computational screen of the National Cancer Institute chemical database.[58] The compound that was initially identified (C1311 or NSC645809) is a known DNA intercalating agent and an inhibitor of FLT3 kinase.[59] This compound, as well as related imidazoacridin-6-ones, inhibits NQO2 in the nanomolar range and is cytotoxic to cells. *N*-Oxide derivatives of the imidazoacridin-6-one compounds that retained nanomolar affinity for NQO2 but had reduced

DNA intercalating properties were developed.[58] Surprisingly, the presence of the *N*-oxide modification also decreased cytotoxicity by 10−20-fold in a variety of cell lines. As such, it appears that the apoptotic effects of this class of inhibitors are due largely to their ability to intercalate DNA. It was also noteworthy that the seven breast cancer cell lines tested in the study exhibited up to 50-fold differences in NQO2 activity but virtually no difference in their sensitivity to the imidazoacridin-6-one inhibitors.[58] The *N*-oxide derivatives of the imidazoacridin-6-one compounds were much less toxic than the parent compounds but still had toxicity IC_{50} values in the low micromolar range; this toxicity was probably not due to inhibition of NQO2, because the IC_{50} values for NQO2 inhibition were typically 2−3 orders of magnitude lower than the toxicity IC_{50} values. That is, for *N*-oxide derivatives of the imidazoacridin-6-one compounds, concentrations that would completely inhibit NQO2 do not appear to be cytotoxic.

From the studies with S29434 and the *N*-oxide derivatives of imidazoacridin-6-one compounds, it appears that inhibition of NQO2 is not cytotoxic; similarly, NQO2 knockout mice were almost identical to wild-type littermates, although there were some differences, including myeloid hyperplasia due to a decreased level of apoptosis of myeloid cells.[57] The NQO2-knockout mice were also more susceptible to benzopyrene-induced carcinogenesis, and the absence of NQO2 prevented TNFα-induced apoptosis in an NFκB-dependent manner.[60,61] In summary, it appears that, on its own, inhibition of NQO2 or genetic knockout is not toxic to cells. Instead, it may be that inhibition or removal of NQO2 in conjunction with other "inputs"—metabolic or oxidative stress, drug-mediated changes in the activity of kinases, DNA damage, and so on—leads to more pronounced toxicity and/or other cellular effects.

Because kinase inhibitors are designed to be kinase specific, the fact that a number of efficacious inhibitors bind NQO2 with high affinity challenges the "single-target" approach in drug discovery. It may be that binding of both NQO2 and kinases is important for the cellular effects of the inhibitors, including enhanced apoptosis of transformed cells. As CK2 and other kinase inhibitors continue to be developed and used as therapeutics, it will be crucial to characterize off-target interactions with NQO2 and possibly other non-kinase targets to fully understand the cellular effects of these compounds and the roles of the individual targets in these effects.

AUTHOR INFORMATION

Corresponding Author

*E-mail: bshilton@uwo.ca. Telephone: (519) 661-4124. Fax: (519) 661-3175.

Funding

This research was supported by an NSERC Discovery Grant to B.H.S. K.K.K.L. is the recipient of an Ontario Graduate Scholarship and a CIHR Doctoral Scholarship.

Notes

The authors declare no competing financial interest.

ABBREVIATIONS

CK2, protein kinase CK2; DMAT, 2-dimethylamino-4,5,6,7-tetrabromo-1*H*-benzimidazole; DYRK, dual-specificity tyrosine-phosphorylated and -regulated kinase; HIPK, homeodomain interacting protein kinase; NQO2, quinone reductase 2; NRH, dihydronicotinamide riboside; PIM, provirus integration site for Moloney murine leukemia virus; S29434, *N*-[2-(2-methoxy-6*H*-dipyrido{2,3-*a*:3,2-*e*}pyrrolizin-11-yl)ethyl]-2-furamide; SCDP, 1-(3-sulfonatopropyl)-3-carbamoyl-1,4-dihydropyrimidine; TBB, 4,5,6,7-tetrabromobenzotriazole; TBBz, 4,5,6,7-1*H*-tetrabromobenzimidazole.

REFERENCES

(1) Zhang, J., Yang, P. L., and Gray, N. S. (2009) Targeting cancer with small molecule kinase inhibitors. *Nat. Rev. Cancer 9*, 28−39.

(2) Meggio, F., and Pinna, L. A. (2003) One-thousand-and-one substrates of protein kinase CK2? *FASEB J. 17*, 349−368.

(3) St-Denis, N. A., and Litchfield, D. W. (2009) Protein kinase CK2 in health and disease: From birth to death: The role of protein kinase CK2 in the regulation of cell proliferation and survival. *Cell. Mol. Life Sci. 66*, 1817−1829.

(4) Filhol, O., and Cochet, C. (2011) Protein kinases curb cell death. *Sci. Signaling 4*, pe26.

(5) Tawfic, S., Yu, S., Wang, H., Faust, R., Davis, A., and Ahmed, K. (2001) Protein kinase CK2 signal in neoplasia. *Histol. Histopathol. 16*, 573−582.

(6) Battistutta, R. (2009) Protein kinase CK2 in health and disease: Structural bases of protein kinase CK2 inhibition. *Cell. Mol. Life Sci. 66*, 1868−1889.

(7) Szyszka, R., Grankowski, N., Felczak, K., and Shugar, D. (1995) Halogenated benzimidazoles and benzotriazoles as selective inhibitors of protein kinases CK I and CK II from *Saccharomyces cerevisiae* and other sources. *Biochem. Biophys. Res. Commun. 208*, 418−424.

(8) Szyszka, R., Boguszewska, A., Shugar, D., and Grankowski, N. (1996) Halogenated benzimidazole inhibitors of phosphorylation, in vitro and in vivo, of the surface acidic proteins of the yeast ribosomal 60S subunit by endogenous protein kinases CK-II and PK60S. *Acta Biochim. Pol. 43*, 389−396.

(9) Sarno, S., Reddy, H., Meggio, F., Ruzzene, M., Davies, S. P., Donella-deana, A., Shugar, D., and Pinna, L. A. (2001) Selectivity of 4,5,6,7-tetrabromobenzotriazole, an ATP site-directed inhibitor of protein kinase CK2 ('casein kinase-2'). *FEBS Lett. 496*, 44−48.

(10) Ruzzene, M., Penzo, D., and Pinna, L. A. (2002) Protein kinase CK2 inhibitor 4,5,6,7-tetrabromobenzotriazole (TBB) induces apoptosis and caspase-dependent degradation of haematopoietic lineage cell-specific protein 1 (HS1) in Jurkat cells. *Biochem. J. 364*, 41−47.

(11) Zień, P., Bretner, M., Zastąpiło, K., Szyszka, R., and Shugar, D. (2003) Selectivity of 4,5,6,7-tetrabromobenzimidazole as an ATP-competitive potent inhibitor of protein kinase CK2 from various sources. *Biochem. Biophys. Res. Commun. 306*, 129−133.

(12) Zień, P., Abramczyk, O., Domańska, K., Bretner, M., and Szyszka, R. (2003) TBBz but not TBBt discriminates between two molecular forms of CK2 in vivo and its implications. *Biochem. Biophys. Res. Commun. 312*, 623−628.

(13) Pagano, M. A., Andrzejewska, M., Ruzzene, M., Sarno, S., Cesaro, L., Bain, J., Elliott, M., Meggio, F., Kazimierczuk, Z., and Pinna, L. A. (2004) Optimization of protein kinase CK2 inhibitors derived from 4,5,6,7-tetrabromobenzimidazole. *J. Med. Chem. 47*, 6239−6247.

(14) Pagano, M. A., Meggio, F., Ruzzene, M., Andrzejewska, M., Kazimierczuk, Z., and Pinna, L. A. (2004) 2-Dimethylamino-4,5,6,7-tetrabromo-1H-benzimidazole: A novel powerful and selective inhibitor of protein kinase CK2. *Biochem. Biophys. Res. Commun. 321*, 1040−1044.

(15) Pagano, M. A., Bain, J., Kazimierczuk, Z., Sarno, S., Ruzzene, M., Di Maira, G., Elliott, M., Orzeszko, A., Cozza, G., Meggio, F., and Pinna, L. A. (2008) The selectivity of inhibitors of protein kinase CK2: An update. *Biochem. J. 415*, 353−365.

(16) Gyenis, L., Kuś, A., Bretner, M., and Litchfield, D. W. (2013) Functional proteomics strategy for validation of protein kinase inhibitors reveals new targets for a TBB-derived inhibitor of protein kinase CK2. *J. Proteomics 81*, 70−79.

(17) Duncan, J. S., Gyenis, L., Lenehan, J., Bretner, M., Graves, L. M., Haystead, T. A., and Litchfield, D. W. (2008) An unbiased evaluation of CK2 inhibitors by chemoproteomics: Characterization of inhibitor

effects on CK2 and identification of novel inhibitor targets. *Mol. Cell. Proteomics 7*, 1077−1088.
(18) Liao, S., Dulaney, J., and William-Ashman, H. (1962) Purification and properties of a flavoprotein catalyzing the oxidation of reduced ribosyl nicotinamide. *J. Biol. Chem. 237*, 2981−2987.
(19) Wu, K., Knox, R., Sun, X. Z., Joseph, P., Jaiswal, A. K., Zhang, D., Deng, P. S., and Chen, S. (1997) Catalytic properties of NAD(P)-H:quinone oxidoreductase-2 (NQO2), a dihydronicotinamide riboside dependent oxidoreductase. *Arch. Biochem. Biophys. 347*, 221−228.
(20) Gong, X., Kole, L., Iskander, K., and Jaiswal, A. K. (2007) NRH:quinone oxidoreductase 2 and NAD(P)H:quinone oxidoreductase 1 protect tumor suppressor p53 against 20s proteasomal degradation leading to stabilization and activation of p53. *Cancer Res. 67*, 5380−5388.
(21) Khutornenko, A. A., Roudko, V. V., Chernyak, B. V., Vartapetian, A. B., Chumakov, P. M., and Evstafieva, A. G. (2010) Pyrimidine biosynthesis links mitochondrial respiration to the p53 pathway. *Proc. Natl. Acad. Sci. U.S.A. 107*, 12828−12833.
(22) Leung, K. K. K., and Shilton, B. H. (2013) Chloroquine binding reveals flavin redox switch function of quinone reductase 2. *J. Biol. Chem. 288*, 11242−11251.
(23) Shen, J., Barrios, R. J., and Jaiswal, A. K. (2010) Inactivation of the quinone oxidoreductases NQO1 and NQO2 strongly elevates the incidence and multiplicity of chemically induced skin tumors. *Cancer Res. 70*, 1006−1014.
(24) Bantscheff, M., Eberhard, D., Abraham, Y., Bastuck, S., Boesche, M., Hobson, S., Mathieson, T., Perrin, J., Raida, M., Rau, C., Reader, V., Sweetman, G., Bauer, A., Bouwmeester, T., Hopf, C., Kruse, U., Neubauer, G., Ramsden, N., Rick, J., Kuster, B., and Drewes, G. (2007) Quantitative chemical proteomics reveals mechanisms of action of clinical ABL kinase inhibitors. *Nat. Biotechnol. 25*, 1035−1044.
(25) Rix, U., Hantschel, O., Dürnberger, G., Remsing Rix, L. L., Planyavsky, M., Fernbach, N. V., Kaupe, I., Bennett, K. L., Valent, P., Colinge, J., Köcher, T., and Superti-Furga, G. (2007) Chemical proteomic profiles of the BCR-ABL inhibitors imatinib, nilotinib, and dasatinib reveal novel kinase and nonkinase targets. *Blood 110*, 4055−4063.
(26) Winger, J. A., Hantschel, O., Superti-Furga, G., and Kuriyan, J. (2009) The structure of the leukemia drug imatinib bound to human quinone reductase 2 (NQO2). *BMC Struct. Biol. 9*, 7.
(27) Brehmer, D., Godl, K., Zech, B., Wissing, J., and Daub, H. (2004) Proteome-wide identification of cellular targets affected by bisindolylmaleimide-type protein kinase C inhibitors. *Mol. Cell. Proteomics 3*, 490−500.
(28) Leung, K. K. K., Litchfield, D. W., and Shilton, B. H. (2012) Flavin adenine dinucleotide content of quinone reductase 2: Analysis and optimization for structure-function studies. *Anal. Biochem. 420*, 84−89.
(29) Kwiek, J. J., Haystead, T. A. J., and Rudolph, J. (2004) Kinetic mechanism of quinone oxidoreductase 2 and its inhibition by the antimalarial quinolines. *Biochemistry 43*, 4538−4547.
(30) Leslie, A. G. W., and Powell, H. R. (2007) Evolving Methods for Macromolecular Crystallography. In *Evolving Methods for Macromolecular Crystallography* (Read, R. J., and Sussman, J. L., Eds.) Vol. *245*, pp 41−51, Springer, Berlin.
(31) Evans, P. (2006) Scaling and assessment of data quality. *Acta Crystallogr. D62*, 72−82.
(32) Foster, C. E., Bianchet, M. A., Talalay, P., Zhao, Q., and Amzel, L. M. (1999) Crystal structure of human quinone reductase type 2, a metalloflavoprotein. *Biochemistry 38*, 9881−9886.
(33) Adams, P. D., Afonine, P. V., Bunkóczi, G., Chen, V. B., Davis, I. W., Echols, N., Headd, J. J., Hung, L.-W., Kapral, G. J., Grosse-Kunstleve, R. W., McCoy, A. J., Moriarty, N. W., Oeffner, R., Read, R. J., Richardson, D. C., Richardson, J. S., Terwilliger, T. C., and Zwart, P. H. (2010) PHENIX: A comprehensive Python-based system for macromolecular structure solution. *Acta Crystallogr. D66*, 213−221.
(34) Politzer, P., Murray, J. S., and Clark, T. (2013) Halogen bonding and other σ-hole interactions: A perspective. *Phys. Chem. Chem. Phys. 15*, 11178−11189.
(35) Levitt, M., and Perutz, M. (1988) Aromatic Rings Act as Hydrogen Bond Acceptors. *J. Mol. Biol. 201*, 751−754.
(36) Hemmerich, P., Nagelschneider, G., and Veeger, C. (1970) Chemistry and molecular biology of flavins and flavoproteins. *FEBS Lett. 8*, 69−83.
(37) Zien, P., Duncan, J. S., Skierski, J., Bretner, M., Litchfield, D. W., and Shugar, D. (2005) Tetrabromobenzotriazole (TBBt) and tetrabromobenzimidazole (TBBz) as selective inhibitors of protein kinase CK2: Evaluation of their effects on cells and different molecular forms of human CK2. *Biochim. Biophys. Acta 1754*, 271−280.
(38) Sarno, S., Salvi, M., Battistutta, R., Zanotti, G., and Pinna, L. A. (2005) Features and potentials of ATP-site directed CK2 inhibitors. *Biochim. Biophys. Acta 1754*, 263−270.
(39) Zanin, S., Borgo, C., Girardi, C., O'Brien, S. E., Miyata, Y., Pinna, L. A., Donella-Deana, A., and Ruzzene, M. (2012) Effects of the CK2 inhibitors CX-4945 and CX-5011 on drug-resistant cells. *PLoS One 7*, e49193.
(40) Guo, C., Gasparian, A. V., Zhuang, Z., Bosykh, D. A., Komar, A. A., Gudkov, A. V., and Gurova, K. V. (2009) 9-Aminoacridine-based anticancer drugs target the PI3K/AKT/mTOR, NF-κB and p53 pathways. *Oncogene 28*, 1151−1161.
(41) Sarno, S., de Moliner, E., Ruzzene, M., Pagano, M. A., Battistutta, R., Bain, J., Fabbro, D., Schoepfer, J., Elliott, M., Furet, P., Meggio, F., Zanotti, G., and Pinna, L. A. (2003) Biochemical and three-dimensional-structural study of the specific inhibition of protein kinase CK2 by [5-oxo-5,6-dihydroindolo-(1,2-a)quinazolin-7-yl]acetic acid (IQA). *Biochem. J. 374*, 639−646.
(42) Battistutta, R., Mazzorana, M., Cendron, L., Bortolato, A., Sarno, S., Kazimierczuk, Z., Zanotti, G., Moro, S., and Pinna, L. A. (2007) The ATP-binding site of protein kinase CK2 holds a positive electrostatic area and conserved water molecules. *ChemBioChem 8*, 1804−1809.
(43) Battistutta, R., Mazzorana, M., Sarno, S., Kazimierczuk, Z., Zanotti, G., and Pinna, L. A. (2005) Inspecting the structure-activity relationship of protein kinase CK2 inhibitors derived from tetrabromo-benzimidazole. *Chem. Biol. 12*, 1211−1219.
(44) Cavelier, G., and Amzel, L. M. (2001) Mechanism of NAD(P)H:quinone reductase: Ab initio studies of reduced flavin. *Proteins 43*, 420−432.
(45) Deininger, M., Buchdunger, E., and Druker, B. J. (2005) The development of imatinib as a therapeutic agent for chronic myeloid leukemia. *Blood 105*, 2640−2653.
(46) Asher, G., Lotem, J., Cohen, B., Sachs, L., and Shaul, Y. (2001) Regulation of p53 stability and p53-dependent apoptosis by NADH quinone oxidoreductase 1. *Proc. Natl. Acad. Sci. U.S.A. 98*, 1188−1193.
(47) Huang, C., Ma, W. Y., Goranson, A., and Dong, Z. (1999) Resveratrol suppresses cell transformation and induces apoptosis through a p53-dependent pathway. *Carcinogenesis 20*, 237−242.
(48) Kim, E. L., Wüstenberg, R., Rübsam, A., Schmitz-Salue, C., Warnecke, G., Bücker, E.-M., Pettkus, N., Speidel, D., Rohde, V., Schulz-Schaeffer, W., Deppert, W., and Giese, A. (2010) Chloroquine activates the p53 pathway and induces apoptosis in human glioma cells. *Neuro-Oncology (Cary, NC, U.S.) 12*, 389−400.
(49) Wendel, H.-G., de Stanchina, E., Cepero, E., Ray, S., Emig, M., Fridman, J. S., Veach, D. R., Bornmann, W. G., Clarkson, B., McCombie, W. R., Kogan, S. C., Hochhaus, A., and Lowe, S. W. (2006) Loss of p53 impedes the antileukemic response to BCR-ABL inhibition. *Proc. Natl. Acad. Sci. U.S.A. 103*, 7444−7449.
(50) Santoro, R., Marani, M., Blandino, G., Muti, P., and Strano, S. (2012) Melatonin triggers p53Ser phosphorylation and prevents DNA damage accumulation. *Oncogene 31*, 2931−2942.
(51) Gurova, K. V., Hill, J. E., Guo, C., Prokvolit, A., Burdelya, L. G., Samoylova, E., Khodyakova, A. V., Ganapathi, R., Ganapathi, M., Tararova, N. D., Bosykh, D., Lvovskiy, D., Webb, T. R., Stark, G. R., and Gudkov, A. V. (2005) Small molecules that reactivate p53 in renal cell carcinoma reveal a NF-κB-dependent mechanism of p53 suppression in tumors. *Proc. Natl. Acad. Sci. U.S.A. 102*, 17448−17453.

(52) Moll, U. M., Wolff, S., Speidel, D., and Deppert, W. (2005) Transcription-independent pro-apoptotic functions of p53. *Curr. Opin. Cell Biol. 17*, 631−636.
(53) Nosjean, O., Ferro, M., Coge, F., Beauverger, P., Henlin, J. M., Lefoulon, F., Fauchere, J. L., Delagrange, P., Canet, E., and Boutin, J. A. (2000) Identification of the melatonin-binding site MT3 as the quinone reductase 2. *J. Biol. Chem. 275*, 31311−31317.
(54) Ferry, G., Hecht, S., Berger, S., Moulharat, N., Coge, F., Guillaumet, G., Leclerc, V., Yous, S., Delagrange, P., and Boutin, J. A. (2010) Old and new inhibitors of quinone reductase 2. *Chem.-Biol. Interact. 186*, 103−109.
(55) Reybier, K., Perio, P., Ferry, G., Bouajila, J., Delagrange, P., Boutin, J. A., and Nepveu, F. (2011) Insights into the redox cycle of human quinone reductase 2. *Free Radical Res. 45*, 1184−1195.
(56) Janda, E., Parafati, M., Aprigliano, S., Carresi, C., Visalli, V., Sacco, I., Ventrice, D., Mega, T., Vadalá, N., Rinaldi, S., Musolino, V., Palma, E., Gratteri, S., Rotiroti, D., and Mollace, V. (2013) The antidote effect of quinone oxidoreductase 2 inhibitor against paraquat-induced toxicity in vitro and in vivo. *Br. J. Pharmacol. 168*, 46−59.
(57) Long, D. J., Iskander, K., Gaikwad, A., Arin, M., Roop, D. R., Knox, R., Barrios, R., and Jaiswal, A. K. (2002) Disruption of dihydronicotinamide riboside:quinone oxidoreductase 2 (NQO2) leads to myeloid hyperplasia of bone marrow and decreased sensitivity to menadione toxicity. *J. Biol. Chem. 277*, 46131−46139.
(58) Dunstan, M. S., Barnes, J., Humphries, M., Whitehead, R. C., Bryce, R. A., Leys, D., Stratford, I. J., and Nolan, K. A. (2011) Novel inhibitors of NRH:quinone oxidoreductase 2 (NQO2): Crystal structures, biochemical activity, and intracellular effects of imidazoacridin-6-ones. *J. Med. Chem. 54*, 6597−6611.
(59) Nolan, K. A., Humphries, M. P., Bryce, R. A., and Stratford, I. J. (2010) Imidazoacridin-6-ones as novel inhibitors of the quinone oxidoreductase NQO2. *Bioorg. Med. Chem. Lett. 20*, 2832−2836.
(60) Ahn, K. S., Gong, X., Sethi, G., Chaturvedi, M. M., Jaiswal, A. K., and Aggarwal, B. B. (2007) Deficiency of NRH:quinone oxidoreductase 2 differentially regulates TNF signaling in keratinocytes: Up-regulation of apoptosis correlates with down-regulation of cell survival kinases. *Cancer Res. 67*, 10004−10011.
(61) Iskander, K., Paquet, M., Brayton, C., and Jaiswal, A. K. (2004) Deficiency of NRH:quinone oxidoreductase 2 increases susceptibility to 7,12-dimethylbenz(a)anthracene and benzo(a)pyrene-induced skin carcinogenesis. *Cancer Res. 64*, 5925−5928.
(62) Battistutta, R., De Moliner, E., Sarno, S., Zanotti, G., and Pinna, L. A. (2001) Structural features underlying selective inhibition of protein kinase CK2 by ATP site-directed tetrabromo-2-benzotriazole. *Protein Sci. 10*, 2200−2206.
(63) Baker, N. A., Sept, D., Joseph, S., Holst, M. J., and McCammon, J. A. (2001) Electrostatics of nanosystems: Application to microtubules and the ribosome. *Proc. Natl. Acad. Sci. U.S.A. 98*, 10037−10041.
(64) Dolinsky, T. J., Czodrowski, P., Li, H., Nielsen, J. E., Jensen, J. H., Klebe, G., and Baker, N. A. (2007) PDB2PQR: Expanding and upgrading automated preparation of biomolecular structures for molecular simulations. *Nucleic Acids Res. 35* (Web Server Issue), W522−W525.
(65) Laskowski, R. A., MacArthur, M., Moss, D. S., and Thorton, J. M. (1993) PROCHECK: a program to check the stereochemical quality of protein structures. *J. Appl. Cryst. 26*, 283−291.